Induction of cyto-protective autophagy by paramontroseite VO$_2$ nanocrystals

Wei Zhou[1], Yanyan Miao[1], Yunjiao Zhang[1], Liang Liu[2], Jun Lin[1], James Y Yang[3], Yi Xie[2] and Longping Wen[1]

[1] Hefei National Laboratory for Physical Sciences at Microscale, and School of Life Sciences, University of Science and Technology of China, Hefei, People's Republic of China
[2] Hefei National Laboratory for Physical Sciences at Microscale, Division of Nanomaterials and Nano-chemistry, University of Science and Technology of China, Hefei, People's Republic of China
[3] School of Life Sciences, Xiamen University, Xiamen, People's Republic of China

E-mail: yxie@ustc.edu.cn and lpwen@ustc.edu.cn

Abstract
A variety of inorganic nanomaterials have been shown to induce autophagy, a cellular degradation process critical for the maintenance of cellular homeostasis. The overwhelming majority of autophagic responses elicited by nanomaterials were detrimental to cell fate and contributed to increased cell death. A widely held view is that the inorganic nanoparticles, when encapsulated and trapped by autophagosomes, may compromise the normal autophagic process due to the inability of the cells to degrade these materials and thus they manifest a detrimental effect on the well-being of a cell. Here we show that, contrary to this notion, nano-sized paramontroseite VO$_2$ nanocrystals (P–VO$_2$) induced cyto-protective, rather than death-promoting, autophagy in cultured HeLa cells. P–VO$_2$ also caused up-regulation of heme oxygenase-1 (HO-1), a cellular protein with a demonstrated role in protecting cells against death under stress situations. The autophagy inhibitor 3-methyladenine significantly inhibited HO-1 up-regulation and increased the rate of cell death in cells treated with P–VO$_2$, while the HO-1 inhibitor protoporphyrin IX zinc (II) (ZnPP) enhanced the occurrence of cell death in the P–VO$_2$-treated cells while having no effect on the autophagic response induced by P–VO$_2$. On the other hand, Y$_2$O$_3$ nanocrystals, a control nanomaterial, induced death-promoting autophagy without affecting the level of expression of HO-1, and the pro-death effect of the autophagy induced by Y$_2$O$_3$. Our results represent the first report on a novel nanomaterial-induced cyto-protective autophagy, probably through up-regulation of HO-1, and may point to new possibilities for exploiting nanomaterial-induced autophagy for therapeutic applications.

S Online supplementary data available from stacks.iop.org/Nano/24/165102/mmedia

(Some figures may appear in colour only in the online journal)

1. Introduction

During autophagy double-membrane structures, termed autophagosomes, sequestrate cytoplasmic contents such as long-lived proteins and damaged organelles. These autophagosomes subsequently fuse with lysosomes to form autolysosomes, leading to the degradation of the engulfed contents by lysosomal enzymes [1, 2]. Autophagy has been demonstrated to play many vital physiological and pathological roles in essentially all mammalian cells [2–7]. While autophagy was once referred to as 'type II programmed cell death', it is now generally recognized that autophagy is not a cell death process, and that the effect of autophagy

on cell fate is complex and sometimes even opposing. The constitutively active basal autophagy, which is present in all cells at all times and is important for intracellular quality control and maintenance of cellular homeostasis, usually plays a protective role and promotes cell survival. On the other hand, an elevated level of autophagy, or induced autophagy, is frequently observed in cells under stress conditions and often promotes cell death. Many physical, chemical and biological factors such as starvation, irradiation, chemotherapeutic treatment and viral infection are known to have the capacity to induce autophagy. With unique physicochemical properties, nanomaterials have emerged as a new class of autophagy-inducers in the recent years [8]. A variety of nanomaterials, such as quantum dots [9, 10], fullerenes [11–13], rare earth oxide and upconversion nanocrystals [14–18], carbon nanotubes [19], gold nanoparticles [20, 21], graphene [22], iron oxide [23], poly(amidoamine) (PAMAM) [24] etc, elicit an autophagic response in the various cell culture systems examined. The autophagy induced by these nanomaterials, in every case that has been carefully studied, promotes cell death [12–14, 16, 23, 24]. This observation has led to the proposition that the autophagy induced by nanomaterials is intrinsically detrimental to cell fate, since the nanomaterials, which are likely to be trapped by the autophagosomes during autophagy but cannot be degraded by lysosomal enzymes in the autolysosomes, may disrupt the normal autophagic process and render the cells prone to death. The pro-death observation for nanomaterial-induced autophagy also raised a new safety concern for engineered nanomaterials, which may enter the human body either unintentionally or deliberately. Indeed, prior studies have shown that PAMAM nanoparticles caused acute lung injury through induction of autophagy [24], and over 50% of the cytotoxicity elicited by rare earth upconversion nanocrystals resulted from the autophagy induced by these nanocrystals [16, 18].

Here we show that, contrary to the pro-death autophagy reported for nanomaterials so far, autophagy induced by paramontroseite VO$_2$ (P–VO$_2$) nanocrystals promotes cell survival. We further show that the pro-survival effect for P–VO$_2$-induced autophagy was manifested through increased expression of heme oxygenase-1 (HO-1), a cellular protein with demonstrated roles in protecting cells against death induced in stress situations. Our results expand upon our current understanding of the autophagic response elicited by nanomaterials and may have significant implications both for biosafety and *in vivo* applications for engineered nanomaterials.

2. Materials and methods

2.1. Reagents

Trehalose, 3-methyladenine and protoporphyrin IX zinc (II) were all purchased from Sigma-Aldrich (St Louis, MO, USA), monodansylcadaverine (MDC), LysoTracker Red and Lipofectamine 2000 were from Invitrogen (Carlsbad, CA, USA), microtubule-associated proteins light chain 3B (LC3) antibody was purchased from Novus (Littleton, CO, USA),

glyceraldehyde phosphate dehydrogenase (GAPDH) antibody was from Chemicon and HO-1 antibody was from Abcam (Cambridge, UK). All cell culture reagents were purchased from Gibco (Carlsbad, CA, USA) and MTT (thiazoyl blue tetrazolium bromide) was from Bio Basic (Markham, Canada).

2.2. Preparation of P–VO$_2$ nanocrystals

P–VO$_2$ was synthesized as previously described [25]. The resulting material was suspended in ultrapure water (pH 6.7; Milli-Q, Bedford, MA, USA) in a concentration of 1 mg ml^{-1} followed by ultrasonic treatment for 4 h in an ultrasonic cleaner (40 kHz, KS150D Ningbo Haishu Kesheng Ultrasonic Equipment Co., Ningbo, China). This aqueous suspension of P–VO$_2$ was irradiated with ultraviolet light in a regular hood for 24 h before use. P–VO$_2$ was characterized by transmission electron microscopy (TEM), performed on a JEOL-2010 high-resolution transmission electron microscope (HRTEM, Tokyo, Japan) at 200 kV.

2.3. MTT assay

HeLa cells were grown in 96-well plates at a density of approximately 10 000 cells per well and then exposed to tested materials or other agents (final volume 0.2 ml per well). At the indicated times, 10 μl of 5 mg ml^{-1} MTT solution in PBS was added to each well and incubated for 4 h. After removal of the medium, 150 μl of DMSO was added to each well to dissolve the formazan crystals. The absorbance at 540 nm was determined using a Biokinetics plate reader (Bio-Tek Instruments, Inc., Winooski, VT, USA). Triplicate wells were assayed for each condition and the standard deviation was determined. The relative cell viability was expressed as a percentage relative to the untreated control cells.

2.4. Cell culture

All cells were continuously cultured as a monolayer at 37 °C and 5% CO$_2$ in Dulbecco's modified Eagle's medium (DMEM; Invitrogen, Karlsruhe, Germany) supplemented with 10% fetal bovine serum, 100 μg ml^{-1} penicillin and 100 μg ml^{-1} streptomycin. HeLa cells were transfected with pGFP-LC3 using Lipofectamine 2000, according to the manufacturer's protocol. Cells were transferred to a new plate and underwent selection in DMEM containing 0.6 mg ml^{-1} of G418 (Promega, Madison, WI, USA) 24 h after transfection, with a change of medium every 3 days. Cell colonies exhibiting strong green fluorescence were selected under a fluorescent microscope 10 days post-transfection and expansion.

2.5. GFP-LC3 dot formation assay

GFP-LC3/HeLa cells were observed by fluorescent microscopy (Olympus IX71, Tokyo, Japan). GFP-LC3 dot formation was quantified by counting 500 cells, and expressed as the ratio between the number of cells with at least

five GFP-LC3 dots and the number of cells with green fluorescence (essentially 100% for our cells stably expressing GFP-LC3). The assays were independently performed by two of the authors in a blinded manner.

2.6. Western blot analysis

After harvesting via trypsinization, the cell pellet was suspended on ice with the lysis buffer (0.5% Nonidet P-40/10 mM Tris-HCl, pH 7.5/100 mM NaCl) supplemented with a protease inhibitor cocktail (Sigma). An equal volume of 2× SDS sample buffer was added, followed by boiling for 10 min. Proteins were separated on a SDS/PAGE gel. The concentration of the gel was 10, 12 or 15% according to the protein that needed to be separated. Then proteins were transferred to a nitrocellulose membrane (Amersham, Freiburg, Germany). After blocking with Tris-buffered saline containing 0.1% Tween-20 and 5% non-fat dry milk, the membrane was incubated for 3 h with a primary antibody at an appropriate dilution in room temperature, extensively washed, incubated with horseradish peroxidase conjugated secondary antibody (1:10 000 dilution) for 1 h, and finally visualized with an enhanced chemiluminescence (ECL) kit (Biological Industries, Beit Haemek, Israel).

2.7. Autophagic marker dye staining

GFP-LC3/HeLa cells, after treatment with P–VO$_2$, were treated with 75 nM LysoTracker Red for 15 min and 10 μM MDC for 30 min, respectively. After washing twice with PBS, the cells were examined by fluorescence microscopy (Olympus IX71, Tokyo, Japan) using different excitation wavelengths according to the manufacturer's instructions.

2.8. Bio-transmission electron microscopy

GFP-LC3/HeLa cells were grown in the six-well plates and treated with nanomaterials for 24 h. After harvesting, the cell pellet was fixed in 0.1 M Na-phosphate buffer (pH 7.4) containing 2% glutaraldehyde for 1 h. After post-fixing in 1% OsO$_4$ at room temperature for 60 min, cells were dehydrated with a graded series of ethanol, and embedded in epoxy resin. Areas containing cells were block mounted and cut into ultrathin sections. The sections were stained with uranyl acetate and lead citrate and examined with a transmission electron microscope (JEOL-1230, Tokyo, Japan).

2.9. Statistical analysis

All data were expressed as mean ± SEM and analyzed by two-tailed Student's *t*-tests.

3. Results

3.1. P–VO$_2$ triggers time- and dose-dependent LC3 dot formation

P–VO$_2$ prepared by us exhibited a rod-like structure approximately 100 nm in length and 10 nm wide (figure 1(a)).

To test the possibility that P–VO$_2$ may induce autophagy, we performed an LC3 dot formation assay in GFP-LC3/HeLa, a HeLa cell line stably expressing GFP-LC3, a fusion protein between green fluorescent protein (GFP) and microtubule-associated light chain 3 (LC3) protein. GFP-LC3 protein is normally present diffusely in the cytosol, but upon autophagy accumulates on the autophagosome membrane and thus appears as green punctate dots in the cell. Treatment with P–VO$_2$ for 12 h resulted in the appearance of many green fluorescent dots in the cell (figure 1(b)). However, P–VO$_2$ did not cause the appearance of large cytosolic vacuoles, a distinct cytotoxic feature unrelated to autophagy that was observed in the cells treated with rare earth (RE) oxide and RE upconversion nanocrystals [17, 18] but no other nanocrystals such as fullerene C60 [12, 13]. P–VO$_2$-mediated GFP-LC3 dot formation was both time- and dose-dependent, with a significant effect observed at 5 μg ml^{-1} for 8 h and near-maximum effect at 5 μg ml^{-1} for 12 h after nanocrystal addition (figure 1(c)). Prolonging treatment still elevated autophagy, but the cell viability was very low as the majority of cells were dead by 96 h.

3.2. P–VO$_2$ induces genuine autophagy

In addition to LC3 dot formation, we conducted several other studies to further prove that P–VO$_2$ induced autophagy. Consistent with enhanced LC3 dot formation, Western blotting with anti-LC3 antibody showed increased conversion of LC3-I to LC3-II in the cells treated with P–VO$_2$, as revealed quantitatively by the normalized LC3-II/GAPDH ratio (figure 2(a)). Staining with MDC, a fluorescent compound commonly used as a tracer for autophagic vacuoles [26], revealed much co-localization with GFP-LC3 dots in P–VO$_2$-treated cells (figure 2(b)). Similar co-localization with GFP-LC3 dots was also observed after staining with LysoTracker Red, a marker dye for lysosomes, suggesting that many of the GFP-LC3 dots were autolysosomes (figure 2(c)). Finally, transmission electron microscopy (TEM) showed that, compared to untreated control cells, HeLa cells treated with 5 μg ml^{-1} P–VO$_2$ for 12 h contained many more autophagic vacuoles (figure 2(d)). Similar autophagic features have been reported for Y$_2$O$_3$ [17]. Collectively, these results strongly support that genuine autophagy is induced in the cells treated with P–VO$_2$.

3.3. Autophagy induced by P–VO$_2$ is pro-survival

To assess the effect of P–VO$_2$-induced autophagy on cell fate, we compared cell viability after P–VO$_2$ treatment in the presence and absence of 3-methyl adenine (3-MA), a widely-used inhibitor of autophagy. P–VO$_2$ was substantially toxic to HeLa cells at concentrations of over 5 μg ml^{-1} (figure 3(a) and figure S1 available at stacks.iop.org/Nano/24/165102/mmedia). 5 mM 3-MA, which effectively inhibited the autophagic response elicited by P–VO$_2$ (figure 3(b)), decreased cell viability by 30% in the cells treated with P–VO$_2$ (figure 3(c)), indicating that autophagy induced by P–VO$_2$ enhanced cell survival. In contrast, 3-MA, which also
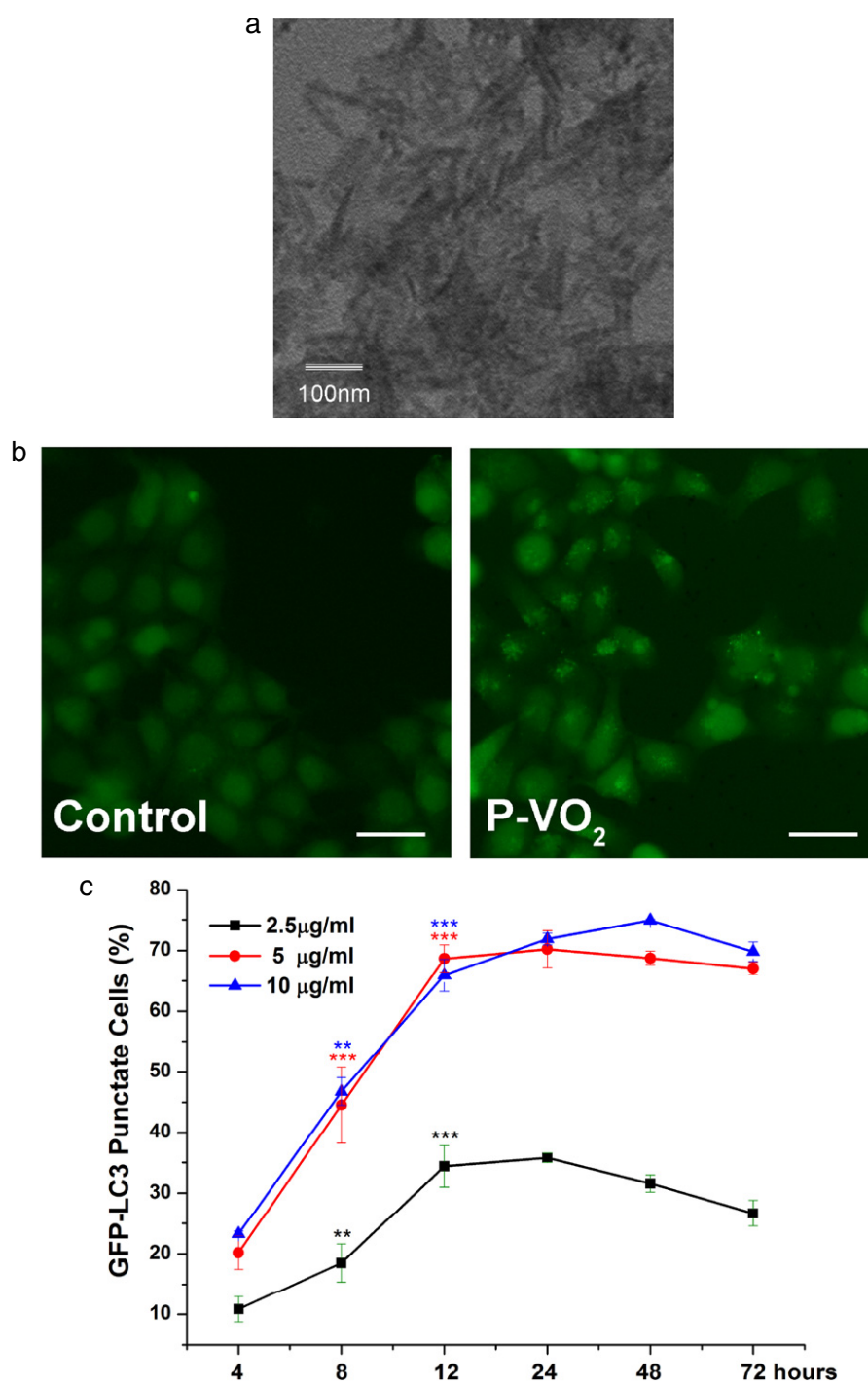
Figure 1. (a) TEM image of P–VO$_2$ (Scale bar = 100 nm). (b) P–VO$_2$ induced GFP-LC3 dot formation in HeLa/LC3 cells. Fluorescent microscopy images of GFP-LC3/HeLa cells treated with 5 μg ml^{-1} VO$_2$ for 12 h. (Scale bar = 20 μm.) (c) Quantified results of punctate GFP-LC3/HeLa cells undergoing P–VO$_2$ treatment in a series of dosages and times (mean $\pm$ SEM, $n = 3$, **$P < 0101$, ***$P < 0.001$).

effectively inhibited Y$_2$O$_3$-induced autophagy (figure 3(b)), enhanced cell viability by 10% in the Y$_2$O$_3$-treated cells (figure 3(c)), in agreement with the published results, indicating that the autophagic response elicited by RE nanocrystals promoted cell death [16, 17]. As a control, 3-MA itself did not alter cell viability. PI/Hoechst results confirmed this pro-survival effect of P–VO$_2$ induced autophagy (figure S2 available at stacks.iop.org/Nano/24/165102/mmedia).

3.4. The pro-survival function of P–VO$_2$-induced autophagy is manifested through HO-1

What is the molecular mechanism underlying the pro-survival effect of P–VO$_2$-induced autophagy? V$_2$O$_3$ nanocrystals have been reported to up-regulate the expression of HO-1 [27], a cytosolic protein with demonstrated roles in protecting against cell death under stress conditions [28–31]. Consistent with
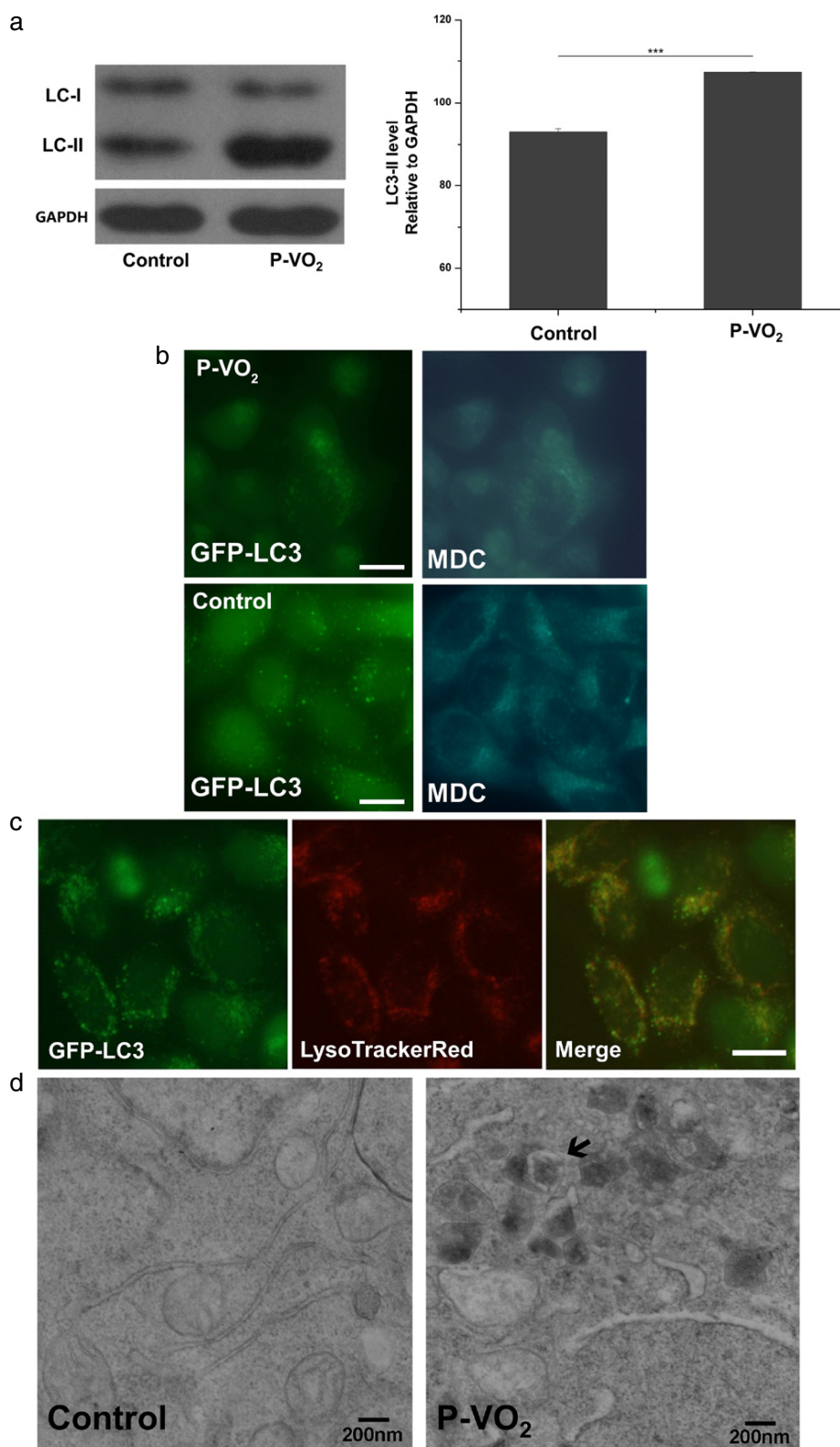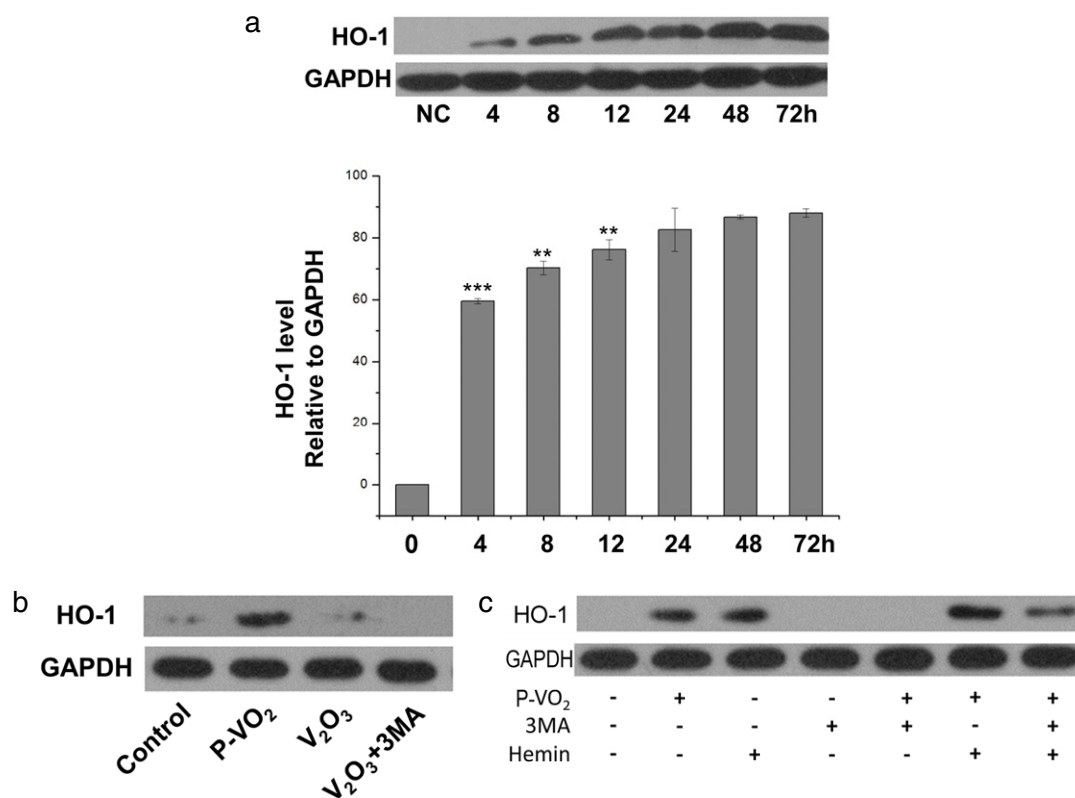
Figure 2. (a) LC3 western blot of HeLa cells treated P–VO$_2$. LC3 Western blot result of HeLa cells that were untreated (Control) or treated with 5 μg ml^{-1} P–VO$_2$. A quantified result is shown in the right panel (mean $\pm$ SEM, $n = 3$, ***$P < 0.001$). (b) MDC stains of GFP-LC3/HeLa cells treated with P–VO$_2$. Fluorescent microscopy images of GFP-LC3/HeLa cells treated with 5 μg ml^{-1}P–VO$_2$ for 12 h and then stained with 10 μM MDC. The GFP-LC3 punctate image is shown in the left and the MDC stain image on the right; images of untreated control are also included in the lower panel. Scale bar $= 20$ μm. (c) LysoTracker Red stains of GFP-LC3/HeLa cells treated with P–VO$_2$. Fluorescent microscopy images of GFP-LC3/HeLa cells treated with 5 μg ml^{-1} P–VO$_2$ for 12 h and then stained with 75 nM LysoTracker Red. The right panel shows the merged image of GFP-LC3 signal (left panel) and the LysoTracker Red stain result (middle panel). Scale bar $= 20$ μm. (d) Bio-TEM images of HeLa cells treated with P–VO$_2$. Cells were incubated with 5 μg ml^{-1} P–VO$_2$ for 12 h. The black arrow shows an autophagosome. Scale bar $= 200$ nm.
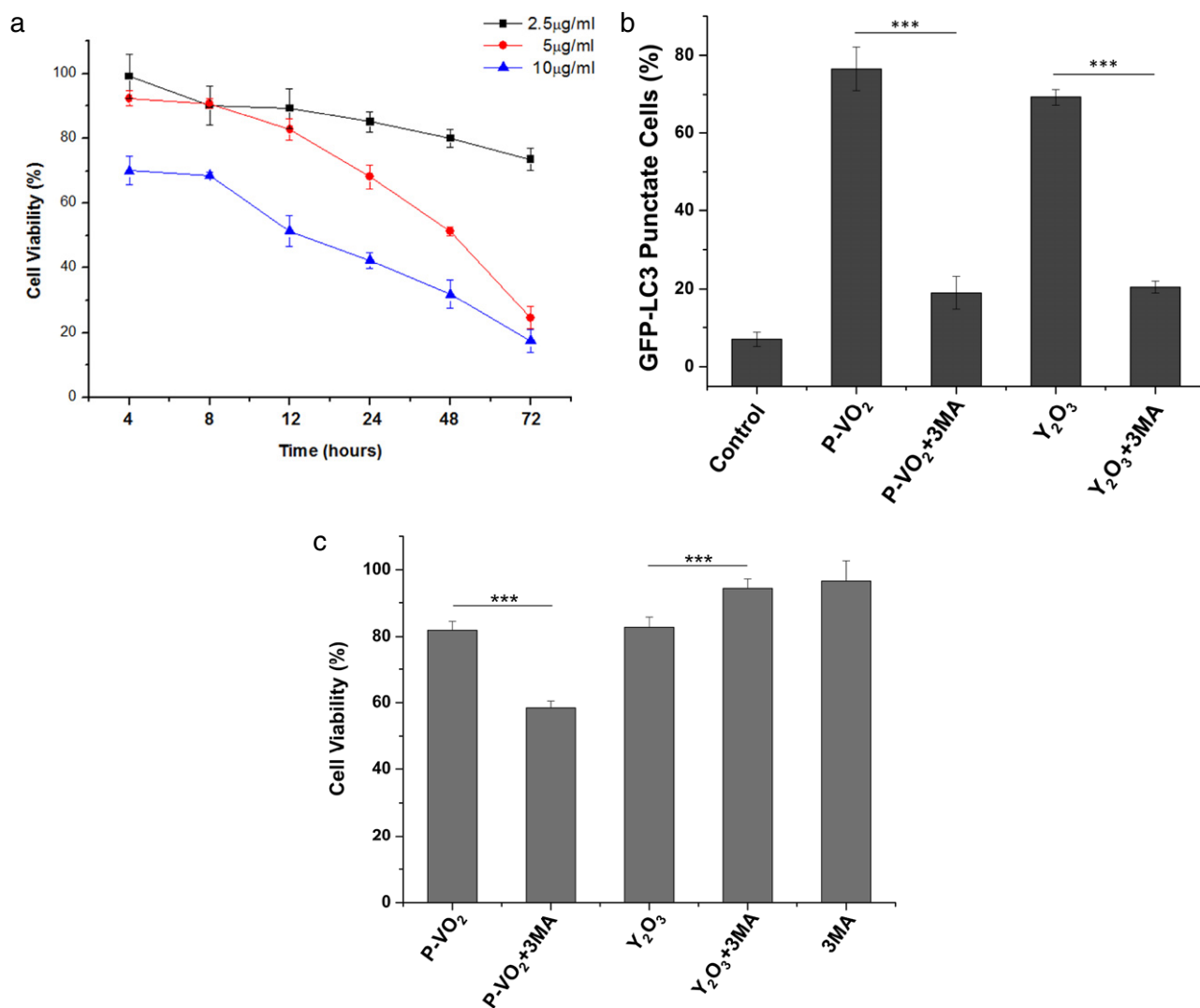
Figure 3. (a) Cell viability result of HeLa cells treated with three different dosages of P–VO$_2$. (b) 3-MA inhibition of autophagy triggered by P–VO$_2$ and Y$_2$O$_3$. The quantified results of GFP-LC3 punctate GFP-LC3/HeLa cells treated with 5 μg ml^{-1} P–VO$_2$ or 30 μg ml^{-1} Y$_2$O$_3$ for 12 h, with or without 5 mM 3-MA (mean $\pm$ SEM, $n = 3$, ***$P < 0.001$). (c) 3-MA increased P–VO$_2$ related cytotoxicity. Cell viability result of HeLa cells treated with 5 μg ml^{-1} P–VO$_2$ or 30 μg ml^{-1} Y$_2$O$_3$ for 12 h, with or without 5 mM 3-MA (mean $\pm$ SEM, $n = 3$, ***$P < 0.001$).

this, P–VO$_2$ dose-dependently increased the HO-1 protein level in HeLa cells. HO-1 up-regulation by P–VO$_2$ followed a similar time course as the induction of autophagy but preceded cell death, as a significant increase in HO-1 was observed at 4 h, and maximum increase at 12 h, after P–VO$_2$ addition (figure 4(a)). In contrast, Y$_2$O$_3$ nanocrystals did not affect HO-1 expression (figure 4(b)). Fullerene C60 and rare earth upconversion nanocrystals, two other types of nanomaterials that induced death-promoting autophagy, also failed to increase HO-1 expression (data not shown). These results prompted us to speculate that HO-1 up-regulation may be the underlying cause for the pro-survival function of P–VO$_2$-induced autophagy. Consistent with this hypothesis, 5 mM 3-MA abolished HO-1 up-regulation by P–VO$_2$ (figure 4(c)), indicating that induction of autophagy was a pre-requisite for enhanced HO-1 expression. More definitive proof for the role of HO-1 in cyto-protective autophagy came

from the studies with the HO-1 inhibitor protoporphyrin IX zinc (II) (ZnPP) and the HO-1 inducer hemin. 10 μM of ZnPP, which effectively inhibited HO-1 enzymatic activity [32], decreased cell viability by 30% in the P–VO$_2$-treated cells (figure 5(a), figure S3 available at stacks.iop.org/Nano/24/165102/mmedia). On the other hand, 20 μM of hemin, which significantly increased the level of HO-1 protein through an autophagy-independent pathway (figure 4(c)), increased cell viability by 25% in the HeLa cells treated with P–VO$_2$ and 3-MA (figure 4(e), figure S4 available at stacks.iop.org/Nano/24/165102/mmedia), indicating that over-expression of HO-1 by hemin was able to rescue cells from the enhanced cytotoxicity imposed by the suppression of cyto-protective autophagy in the P–VO$_2$-treated cells. ZnPP and hemin themselves had a minimal effect on the cell viability (figure 5(b)), did not induce autophagy, and had no effect on the autophagy induced by P–VO$_2$ (figure 5(c)). Collectively,

Figure 4. (a) P–VO$_2$ induced HO-1 expression. HO-1 Western blot of untreated HeLa cells or HeLa cells incubated with 5 μg ml^{-1} P–VO$_2$ for 4–72 h. The lower panel shows the quantified results (mean $\pm$ SEM, $n = 3$, **$P < 0.01$, ***$P < 0.001$, comparison is between sample value and previous time point). (b) Y$_2$O$_3$ had no impact on HO-1 expression. HO-1 Western blot of untreated HeLa cells or HeLa cells treated with 5 μg ml^{-1} P–VO$_2$ or 30 μg ml^{-1} Y$_2$O$_3$ for 12 h, with or without 5 mM 3-MA. (c) 3-MA abolished P–VO$_2$ induced HO-1 expression. HO-1 Western blot of HeLa cells treated with 5 μg ml^{-1}P–VO$_2$ only or alone with 20 μM hemin, 50 mM ZnPP or/and 5 mM 3MA for 12 h.

the above results demonstrated that the autophagy induced by P–VO$_2$ is cyto-protective due to the unique ability of P–VO$_2$ to up-regulate the expression of HO-1. A schematic illustration for the action of P–VO$_2$ and other nanocrystals such as Y$_2$O$_3$ is shown in figure 6.

4. Discussion and conclusion

In this paper we have provided comprehensive evidence concerning P–VO$_2$ induced autophagy. In particular, autophagy induced by P–VO$_2$ played a pro-survival role, as the inhibition of autophagy decreased cell viability and increased the cytotoxicity of P–VO$_2$, even though the autophagy induced by P–VO$_2$ was able to sustain cell survival for only a limited extent and was unable to alter the ultimate fate of the cells after prolonged exposure to P–VO$_2$. To our knowledge, this represents the first report that autophagy induced by a nanomaterial is able to exert a positive effect on cell fate. A great variety of nanomaterials have shown an autophagy-inducing capability, and in all of the cases where the role of autophagy induction on cell fate was evaluated, the elevated autophagy promoted cell death. These findings have led to the suggestion that the autophagy induced by nanomaterials in general is detrimental to cells and represents an emerging safety concern for engineered nanomaterials, which may enter the human body either spontaneously

or intentionally. While that notion remains valid, P–VO$_2$ provided an intriguing exception and illustrated the need to study the autophagy-modulating effects of nanomaterials in a systematic fashion. On the other hand, the fact that autophagy induced by nanomaterials could be pro-survival opens up new possibilities for the biomedical applications of nanomaterials, as the autophagic response in target cells (such as neurons and antigen-presenting cells) may be exploited to enhance clearance of intracellular protein aggregates or increase the efficiency of antigen presentation [11, 33].

We also showed that the pro-survival function of P–VO$_2$-induced autophagy was mediated through up-regulation of HO-1, a low-molecular-weight stress protein which serves a vital metabolic function as the rate-limiting step in the heme degradation pathway and in the maintenance of iron homeostasis [34–36]. HO-1 is also an important cellular protective arbitrator protein and confers protection against cell death in many stress situations such as oxidative stress, hypoxia and cytokine stress [35–38]. Notably, up-regulation of HO-1 expression by P–VO$_2$ was a consequence, rather than an independent event, of autophagy induction, as inhibition of autophagy by 3-MA significantly inhibited HO-1 up-regulation. In contrast, Y$_2$O$_3$ nanocrystals, which induced death-promoting autophagy, did not cause HO-1 up-regulation. Thus the autophagy induced by P–VO$_2$ is
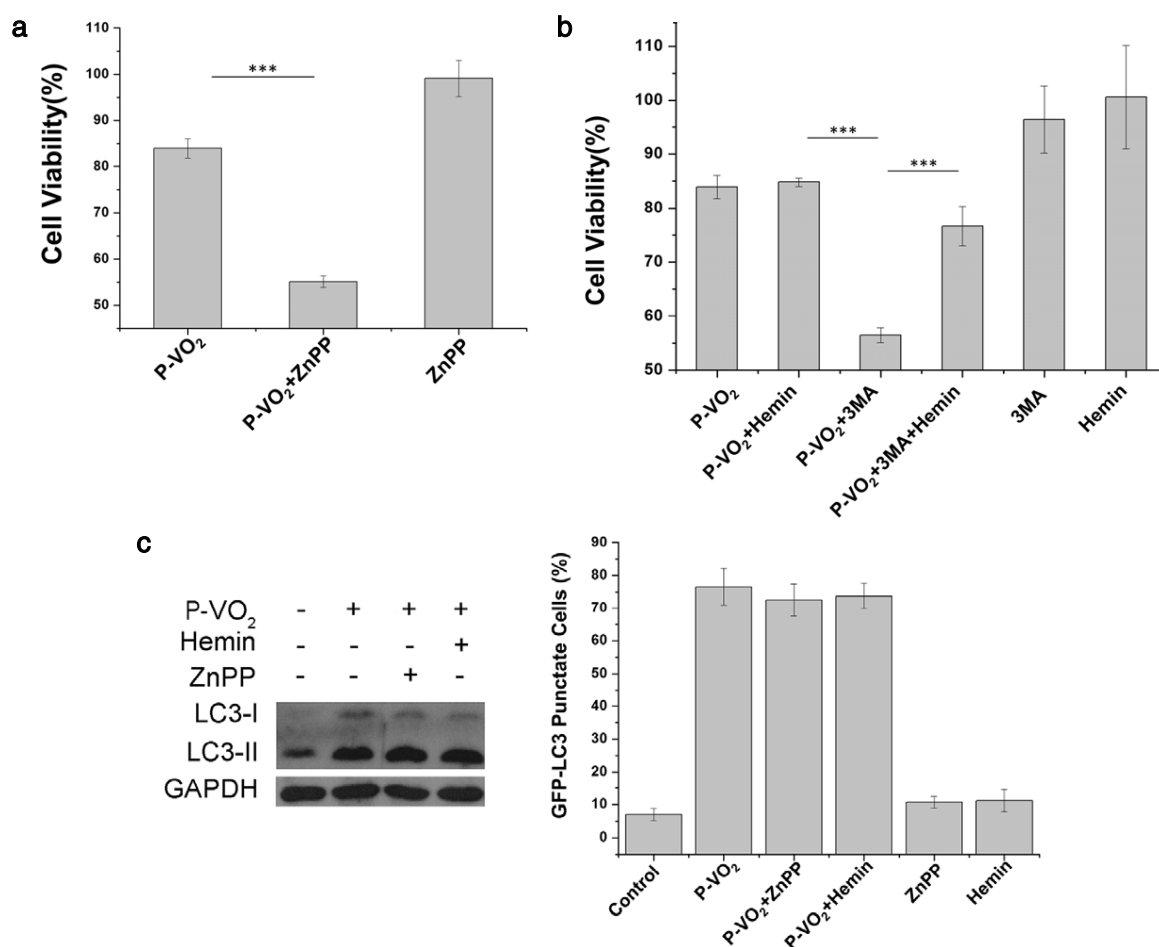
Figure 5. (a) ZnPP decreased the viability of cells treated with P–VO$_2$. MTT results for cells incubated with 5 μg ml^{-1} P–VO$_2$, 5 μg ml^{-1} P–VO$_2$ together with 50 mM ZnPP, or 50 mM ZnPP only for 12 h (mean $\pm$ SEM, $n = 3$, ***$P < 0.001$). (b) Hemin rescued cells incubated with P–VO$_2$ from 3-MA enhanced loss of cell viability. MTT result for cells treated with 5 μg ml^{-1} P–VO$_2$, in addition with 20 μM hemin, 50 mM ZnPP or 5 mM 3-MA. (c) ZnPP and hemin have no influence on P–VO$_2$ induced autophagy. LC3 Western blot result for HeLa cells (left) and quantified results of GFP-LC3 punctate GFP-LC3/HeLa cells treated with 5 μg ml^{-1} P–VO$_2$ (right), in addition with 20 μM hemin or 50 mM ZnPP.
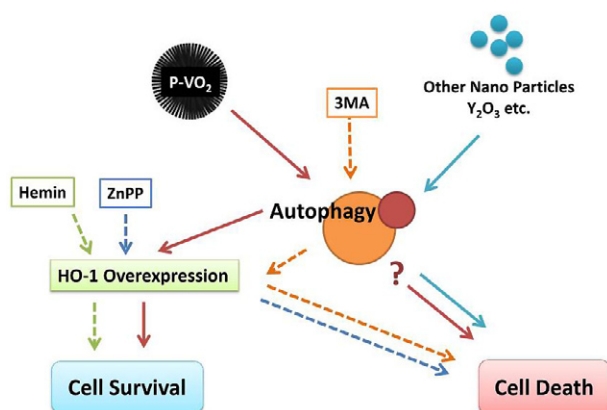
Figure 6. Schematic illustration of the action of P–VO$_2$ and other nanocrystals such as Y$_2$O$_3$. Dashed lines indicate the response of inhibitors or activators while the solid lines indicate biological processes triggered by nanoparticles.

unique in its ability to enhance HO-1 expression. It remains to be shown why the autophagy induced by P–VO$_2$ led to HO-1 up-regulation while the autophagy induced by other nanocrystals did not. The physicochemical properties of different types of nanomaterials ar likely to play critical roles for these autophagic responses. Our results also suggested that HO-1 up-regulation may be an effective means to mitigate nanomaterial toxicity resulted from induction of death-promoting autophagy, and inducers of HO-1 expression may be useful to enhance the biosafety of engineered nanomaterials and nanodevices.

Acknowledgments

References

[1] Glick D, Barth S and Macleod K F 2010 Autophagy: cellular and molecular mechanisms *J. Pathol.* **221** 3–12

[2] Maiuri M C, Zalckvar E, Kimchi A and Kroemer G 2007 Self-eating and self-killing: crosstalk between autophagy and apoptosis *Nature Rev. Mol. Cell Biol.* **8** 741–52

[3] Kondo Y, Kanzawa T, Sawaya R and Kondo S 2005 The role of autophagy in cancer development and response to therapy *Nature Rev. Cancer* **5** 726–34

[4] Levine B, Mizushima N and Virgin H W 2011 Autophagy in immunity and inflammation *Nature* **469** 323–35

[5] Rabinowitz J D and White E 2010 Autophagy and metabolism *Science* **330** 1344–8

[6] Rubinsztein D C, Marino G and Kroemer G 2011 Autophagy and aging *Cell* **146** 682–95

[7] Shintani T and Klionsky D J 2004 Autophagy in health and disease: a double-edged sword *Science* **306** 990–5

[8] Zabirnyk O, Yezhelyev M and Seleverstov O 2007 Nanoparticles as a novel class of autophagy activators *Autophagy* **3** 278–81

[9] Seleverstov O *et al* 2006 Quantum dots for human mesenchymal stem cells labeling. A size-dependent autophagy activation *Nano Lett.* **6** 2826–32

[10] Stern S T, Zolnik B S, McLeland C B, Clogston J, Zheng J and McNeil S E 2008 Induction of autophagy in porcine kidney cells by quantum dots: a common cellular response to nanomaterials? *Toxicol. Sci.* **106** 140–52

[11] Lee C M, Huang S T, Huang S H, Lin H W, Tsai H P, Wu J Y, Lin C M and Chen C T 2011 C60 fullerene–pentoxifylline dyad nanoparticles enhance autophagy to avoid cytotoxic effects caused by the beta-amyloid peptide *Nanomedicine* **7** 107–14

[12] Wei P, Zhang L, Lu Y, Man N and Wen L 2010 C60(Nd) nanoparticles enhance chemotherapeutic susceptibility of cancer cells by modulation of autophagy *Nanotechnology* **21** 495101

[13] Zhang Q, Yang W, Man N, Zheng F, Shen Y, Sun K, Li Y and Wen L P 2009 Autophagy-mediated chemosensitization in cancer cells by fullerene C60 nanocrystal *Autophagy* **5** 1107–17

[14] Chen Y, Yang L, Feng C and Wen L P 2005 Nano neodymium oxide induces massive vacuolization and autophagic cell death in non-small cell lung cancer NCI-H460 cells *Biochem. Biophys. Res. Commun.* **337** 52–60

[15] Man N, Yu L, Yu S H and Wen L P 2010 Rare earth oxide nanocrystals as a new class of autophagy inducers *Autophagy* **6** 310–1

[16] Yu L, Lu Y, Man N, Yu S H and Wen L P 2009 Rare earth oxide nanocrystals induce autophagy in HeLa cells *Small* **5** 2784–7

[17] Zhang Y, Yu C, Huang G, Wang C and Wen L 2010 Nano rare-earth oxides induced size-dependent vacuolization: an independent pathway from autophagy *Int. J. Nanomed.* **5** 601–9

[18] Zhang Y *et al* 2012 Tuning the autophagy-inducing activity of lanthanide-based nanocrystals through specific surface-coating peptides *Nature Mater.* **11** 817–26

[19] Liu H L *et al* 2011 A functionalized single-walled carbon nanotube-induced autophagic cell death in human lung cells through Akt-TSC2-mTOR signaling *Cell Death Dis.* **2** e159

[20] Li J J, Hartono D, Ong C N, Bay B H and Yung L Y 2010 Autophagy and oxidative stress associated with gold nanoparticles *Biomaterials* **31** 5996–6003

[21] Wu Y N *et al* 2011 The selective growth inhibition of oral cancer by iron core-gold shell nanoparticles through mitochondria-mediated autophagy *Biomaterials* **32** 4565–73

[22] Markovic Z M *et al* 2012 Graphene quantum dots as autophagy-inducing photodynamic agents *Biomaterials* **33** 7084–92

[23] Khan M I, Mohammad A, Patil G, Naqvi S A, Chauhan L K and Ahmad I 2012 Induction of ROS, mitochondrial damage and autophagy in lung epithelial cancer cells by iron oxide nanoparticles *Biomaterials* **33** 1477–88

[24] Li C *et al* 2009 PAMAM nanoparticles promote acute lung injury by inducing autophagic cell death through the Akt-TSC2-mTOR signaling pathway *J. Mol. Cell Biol.* **1** 37–45

[25] Wu C, Hu Z, Wang W, Zhang M, Yang J and Xie Y 2008 Synthetic paramontroseite VO$_2$ with good aqueous lithium-ion battery performance *Chem. Commun.* 3891–3

[26] Klionsky D J *et al* 2008 Guidelines for the use and interpretation of assays for monitoring autophagy in higher eukaryotes *Autophagy* **4** 151–75

[27] Wörle-Knirsch J M, Kern K, Schleh C, Adelhelm C, Feldmann C and Krug H F 2007 Nanoparticulate vanadium oxide potentiated vanadium toxicity in human lung cells *Environ. Sci. Technol.* **41** 331–6

[28] Choi A and Alam J 1996 Heme oxygenase-1: function, regulation, and implication of a novel stress-inducible protein in oxidant-induced lung injury *Am. J. Respir. Cell Mol. Biol.* **15** 9–19

[29] Inoue M, Tazuma S, Hyogo H, Nonaka M, Iwamoto K, Nabeshima Y, Ishitobi T, Igarashi K and Chayama K 2007 Heme oxygenase-1 (HO-1), a physiological anti-oxidant, uniquely prevents lipid accumulation in the liver. A novel aspect on the pathogenic role of oxidative stress in nonalcoholic steatohepatitis (NASH) *Gastroenterology* **132** A820-A

[30] Poss K D and Tonegawa S 1997 Reduced stress defense in heme oxygenase 1-deficient cells *Proc. Natl Acad. Sci. USA* **94** 10925–30

[31] Yang Y *et al* 2003 Selective protection of renal tubular epithelial cells by heme oxygenase (HO)-1 during stress-induced injury *Kidney Int.* **64** 1302–9

[32] Gonzalez-Michaca L, Farrugia G, Croatt A J, Alam J and Nath K A 2004 Heme: a determinant of life and death in renal tubular epithelial cells *Am. J. Physiol. Renal Physiol.* **286** F370–7

[33] Li H, Li Y, Jiao J and Hu H M 2011 Alpha-alumina nanoparticles induce efficient autophagy-dependent cross-presentation and potent antitumour response *Nature Nanotechnol.* **6** 645–50

[34] Kikuchi G, Yoshida T and Noguchi M 2005 Heme oxygenase and heme degradation *Biochem. Biophys. Res. Commun.* **338** 558–67

[35] Yoshida T and Migita C T 2000 Mechanism of heme degradation by heme oxygenase *J. Inorg. Biochem.* **82** 33–41

[36] Chepelev N L and Willmore W G 2011 Regulation of iron pathways in response to hypoxia *Free Radical Biol. Med.* **50** 645–66

[37] Lin Q *et al* 2007 Heme oxygenase-1 protein localizes to the nucleus and activates transcription factors important in oxidative stress *J. Biol. Chem.* **282** 20621–33

[38] Yang C M, Lee I T, Luo S F, Lee C W, Wang S W, Lin C C, Chang C C, Chen Y L and Chau L Y 2009 Overexpression of HO-1 protects against TNF-alpha-mediated airway inflammation by down-regulation of TNFR1-dependent oxidative stress *Am. J. Pathol.* **175** 519–32